LAWRENCE
LIVERMORE
NATIONAL
LABORATORY

LLNL-JRNL-818694

Confinement effects of the solvated alkaline metal cation in 1T-MoS2 channel: a First-principles study

C. Zhan, Y. Sun, F. Aydin, Y. Wang, A. Pham

January 25, 2021

Journal of Chemical Physics

Disclaimer

Confinement effects on the solvation structure of solvated alkaline metal cations in a single-digit 1T-MoS_2 nanochannel: A first-principles study

Cheng Zhan*[1], Yangyunli Sun[3], Fikret Aydin[1], Y. Morris Wang[2], Tuan Anh Pham*[1]

[1]Material Science Division, Lawrence Livermore National Laboratory, Livermore, CA, 94550, United States

[2]Department of Materials Science and Engineering, University of California, Log Angeles, CA, 90095, United States

[3]Department of Chemistry, University of California, Riverside, CA, 92521, United States

Corresponding author: zhan1@llnl.gov; pham16@llnl.gov

Abstract: Confinement plays an important role in determining ion transport in porous materials, which in turn may influence the performance of many energy storage and desalination devices. In this work, we combined density functional theory (DFT) with implicit solvation model and *ab initio* molecular dynamics (AIMD) to investigate the effects of nanoconfinement on several solvated alkaline metal cations in a single-digit 1T-MoS_2 nanochannel. Our DFT calculations with a solvation model indicated that cations with a stronger hydration energy introduce a higher number of co-intercalated water molecules into the channel, consistent with early experimental observation obtained for MXene (2D transition metal carbide) channels. The predicted optimal water numbers for the cations were then used for AIMD simulations that explicitly include the effects of solvent. When compared with the cations in bulk solution, our simulations showed that the hydration structure and coordination number (CN) of the solvated cations confined in the MoS_2 channel can be significantly altered. We found that larger cations with a weaker hydration energy (K^+, Rb^+, and Cs^+) exhibited a distinctive CN decrease under confinement, while smaller cations (Li^+, and Na^+) retain a similar hydration shell as in the bulk solution. More specifically, the hydration shell of large cations (K^+, Rb^+, Cs^+) in MoS_2 showed similar feature of coordination angle to the bulk, which suggests the partially brokened hydration shell with no geometry change under confinement. Our simulations provided insights into the change of the hydration structure of alkaline metal cations under confinement, which may have important implication on their transport in the 1T-MoS_2 channel.

Introduction:

Ion transport under nanoconfinement is central to many energy and environmental technologies, such as capacitive energy storage and ion separation.[1-4] In these devices, achieving fundamental understanding of confinement effects on ions in nanopores is essential for material design and optimization for improved performance. Early studies have revealed the importance of confinement in nano-scale energy storage; for example, enhancement in the capacitive performance was observed experimentally by Largeot *et al.* for sub-nanometer carbon nanopores with ionic liquids.[5] The mechanism of this confinement-induced capacitance enhancement has been discussed using molecular simulations by Feng *et al.*[6] and Jiang *et al.*[7], who proposed an

oscillating behavior of the capacitance as a function of the pore size, and suggested the optimal pore size for specific ionic liquids. Besides ionic liquids, confinement effects of aqueous solution in carbon-based nanopores also has been widely studied via classical molecular dynamics simulations. For instance, Kalluri *et al.* investigated the ion partition and hydration structure of NaCl aqueous solution in graphene slit-pores with a varied surface charge density.[8] In addition, Dai *et al.* studied the ion transport in graphene oxide nano-channels, showing that interfacial friction plays an important role in determining ion and water transport within the channels.[9]

Besides carbon-based membranes and nano-channels, layered 2D materials have been reported as promising alternatives for capacitive energy storage and ion separation.[10-14] However, unlike carbon-based systems, such as graphene slit-pores and carbon nanotubes, that have been extensively investigated by molecular dynamics simulations, theoretical simulation of hydrated ion in MoS_2 channel remains limited. One of the major challenge is related to the need of reliable force-fields for the description of the interaction between ion/water and ion/MoS_2 for confined systems, although a set of classical force-field parameter was proposed in recent years to describe the interaction between water and MoS_2 surfaces.[15] In addition, the hydrophobicity/hydrophilicity nature of 2D material surface may affect the density of confined water in sub-nanometer channels, depending on the ion type. This phenomenon has been experimentally probed by Shpigel *et al.* for MXene channels,[16] where the authors show that a significant difference in the hydration structure between confined ions and those in the bulk may exist, which may have an important impact on the transport behavior. In this regard, a reliable estimate of the water density in nano-channels with intercalated ions is needed; in addition, the results can be used as an input for *ab initio* molecular dynamics (AIMD) simulations for further investigation of confined ions.

In this work, we combined density functional theory (DFT) calculation with three-dimensional reference interaction site model (RISM) to investigate hydrated cations, including Li^+, Na^+, K^+, Rb^+, and Cs^+ confined in a single-digit 1T-MoS_2 nanochannel. We focused on the channel with a width around 1 nm that represents a strong confinement limit. In particular, we computed the optimal water number for a 1.1 nm-width MoS_2 channel (the width is defined by the sulfur-sulfur interlayer distance) with different cations using the DFT-RISM approach, which has been utilized for determining the water density in MXene channel[17] and zeolite.[18] We note that the width of the channel investigated here is comparable to the one employed in Ref.[12], where MoS_2 was used as supercapacitor electrode materials. This optimal water density was then used as input for setting AIMD simulations with explicit water molecules to probe confinement effects on the hydration structure of the ions in an ideal channel with an infinite length in the *xy* plane. Our calculation shows that the water density in the MoS_2 channel can strongly depends on the intrinsic properties of the ions. In addition, AIMD simulations provide atomistic details of the hydration structure of the cations under confinement; in particular, we show that the ion solvation in MoS_2 channels can exhibit significant variation from the behavior found in the bulk solution depending on the strength of the ion hydration.

Simulation methods:

Density functional theory (DFT) with a reference interaction site model (RISM)[18] implemented in the Quantum Espresso package[19] was used to compute the total solvation energy of a solvated

cation-MoS_2 channel system to search the optimal water density. In this calculation, the MoS_2 channel and an explicit cation (Figure 1a) was treated by DFT, while confined water in the channel was implicitly treated by RISM, as shown by the colored medium in Figure 1b. The exchange and correlation interactions in DFT were treated at the level of the generalized gradient approximation using the Perdew–Burke–Ernzerhof exchange–correlation functional (GGA-PBE).[20] Optimized norm-conserving Vanderbilt pseudopotentials (ONCV) were used to describe the nuclei-electron interaction with the plane-wave basis set.[21] The cutoff energy of planewave basis was 40 Ry and the k-point sampling in Brillouin zone is gamma point only. The convergence criteria for structure optimization and single point calculation were set to 10^{-3} Ry/Bohr and 10^{-6} Ry, resepectively.

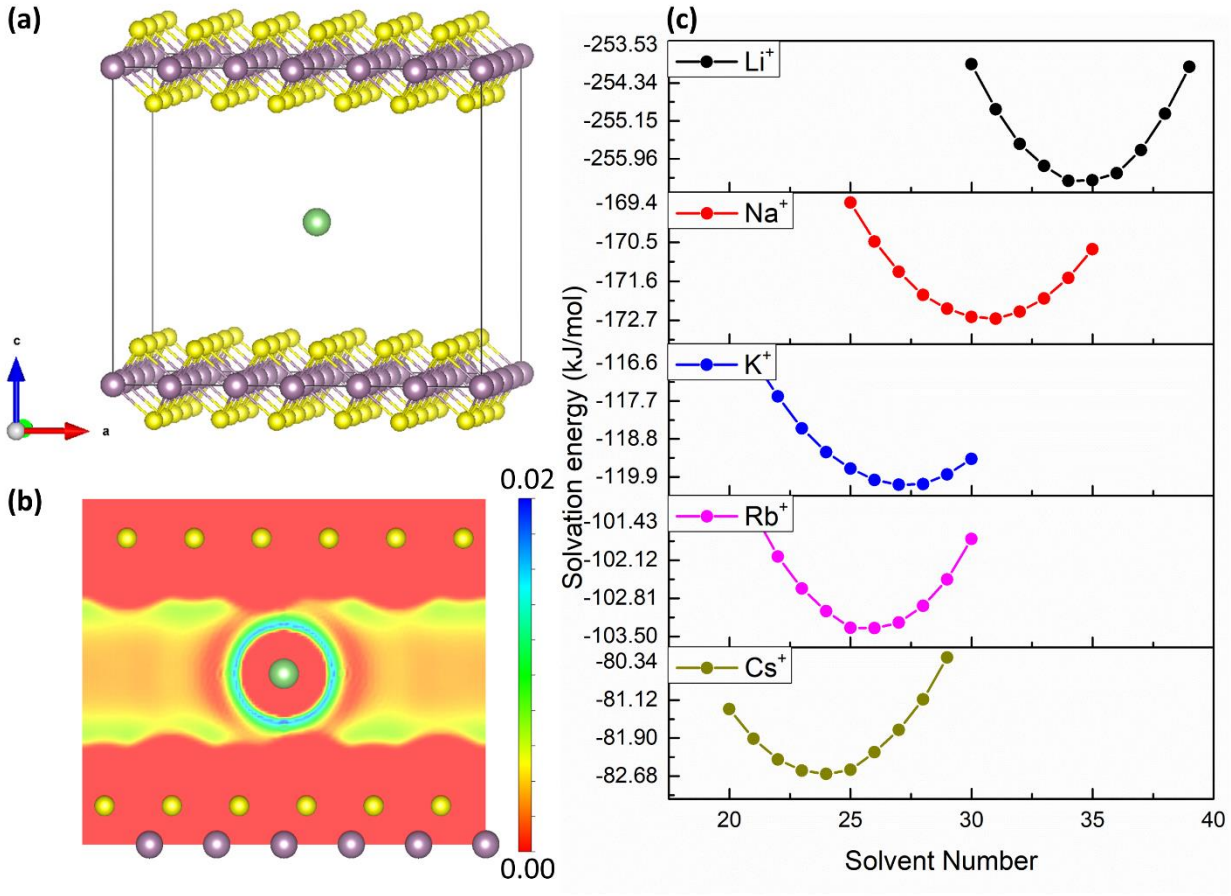

Figure 1. (a) Simulation cell of 1T-MoS_2 channel with one explicit ion; (b) Schematic description of the DFT-RISM calculation of a solvated cation confined in MoS_2 channel filled with implicit solvation of water (color bar refers to the local density of oxygen site in H_2O molecule); (c) Prediction of the optimal water density in a 1.1 nm-width MoS_2 channel with different cations from the calculation of the solvation energy of the cation-MoS_2 system as a function of the water number.

The implicit solvation was described by the RISM approach with the closure model proposed by Kovalenko and Hirata.[22] In addition, the Lennard-Jones (LJ) potentials of the single-point-charge (SPC) water model[23] was used for the solvent, while those of ions and MoS_2 were obtained from the optimized potentials for liquid simulations all-atom (OPLSAA) force fields[22] and earlier MD simulations.[15] Our 1T-MoS_2 channel was modeled by an orthorhombic cell including 24 Mo and 48 S with the lattice parameter of A=16.575 Å, B=12.76 Å and C=14.15 Å (Figure 1a). The approximate channel size was ~1.1 nm determined by sulfur-sulfur distance, which is comparable to the measured interlayer space of a Li^+ intercalated 1T-MoS_2.[12] Considering the different hydration energy of different cations, the optimal water number was obtained by searching the minimum of solvation energy with various solvent number in the channel, as shown in Figure 1c. After the optimal water number was obtained, the corresponding number of explicit water molecules were introduced into the MoS_2 nanopore using the PACKMOL software[24] for further first-principles molecular dynamics simulation. In addition, we also computed the solvation free energy of an individual cation in a 40×40×40 $Å^3$ cubic box in comparison with experimental data[25] in Table S1, where we found that the use of the atomic charge and LJ parameters of the OPLSAA force fields underestimates the solvation free energy compared with experimental data. This discrepancy can be reduced by modifying the LJ parameters, and we found that this leads to a small change in the optimal water number. Moreover, the exchange-correlation functional was also found to have a little impact on the solvation energy of the ion (see Table S2 for Li^+). Based on these tests, we validated the feasibility of predicting the optimal water number via DFT-RISM calculation.

Ab initio molecular dynamics (AIMD) simulations was performed using the Vienna Ab initio Simulation Package (VASP).[26] Here, the exchange-correlation interaction was described by the Generalized-Gradient-Approximation with the Perdew-Burke-Ernzerhof (PBE) formalism.[20] Projector augmented wave (PAW) potential was used to treat the nuclei-electron interaction.[27] The energy cutoff of the planewave basis set was set to 400 eV, and the Brillouin zone was sampled by the Γ point only. The AIMD simulations were carried out using the Nosé-thermostat at 400 K for 60 ps with a time step of 0.5 fs.[28-30] An elevated temperature was chosen as the use of a simulation temperature of around 400 K and the PBE functional has been shown to recover experimental ion solvation structure, as well as water structure and diffusion coefficient at ambient conditions.[31-33] To test our simulation protocol, we also carried out additional simulation of Li^+ at 300 K using revPBE-D3 that includes dispersion correction, where we show that the two simulation yield consistent results for the solvation structure of the ion under confinement (Figure S1). For the structural analysis, we used statistics collected from 50 ps trajectories after the systems were equilibrated for at least 10 ps. In addition, five parallel 60-ps-MD simulations were performed for each cations to improve the statistics of the calculations. For comparison, AIMD simulations of 60 ps were carried out for the same cations in bulk water, where we used one ion in a cubic water box (9.957 Å) with 33 water molecules. The calculation of density profile and radial distribution function (RDF) were conducted using the TRAVIS software.[34] Considering the possible change of coordination number under confinement, we computed the angular distribution function (ADF) defined as:

$$\rho(\alpha) = \frac{1}{N_{image}} \sum_{i=i}^{i=CN} \sum_{j=i+1}^{j=CN} < \delta(\alpha - \angle(\vec{r}_i, \vec{r}_j)) >_t \quad (|\vec{r}| < R_{cut}) \tag{1}$$

CN refers to the coordination number defined by the number of M-O pair within the cutoff distance R_{cut}; the latter was defined by the location of first minimum in the ion-oxygen RDF of the ion in the bulk solution. Here, $\vec{r}_i$ is the vector from cation to oxygen with the index *i*. In this way, the calculated ADF represents the image-averaged number of coordination angle $\angle(\vec{r}_i, \vec{r}_j) = \alpha$ over time; this is different from the probability of finding the coordination angle at α, since $\rho(\alpha)$ also depends on the CN of the ion.

Results and Discussion:

To quantify the optimal number of water molecules in the MoS_2 channel with an intercalated cation, we computed the total solvation energy of the system as a function of the water number using the DFT-RISM method. As shown in Figure 1c, the optimal water number for different alkaline metal cations was found to be 34, 30, 26, 25, 23 for Li^+, Na^+, K^+, Rb^+ and Cs^+, respectively. These differences in the water number are due to the variation in the hydration and ionic sizes of the ions. Specifically, small cations with a larger hydration energy occupy less space in the channel but carrying a higher number of water molecules, and the opposite scenario was found for the larger cations. Interestingly, similar phenomenon has been experimentally observed for layered MXene channels by Shpigel *et al.*, who found that a large cation (K^+) introduces less co-intercalated water molecules than a smaller one (Li^+).[16] As we showed in our previous studies, water exclusion and co-intercalation can have significant impacts on the ion intercalation barrier into the nanopores.[35] These findings also pointed to the importance of having a reliable estimate of the water density under nano-confinement for investigating ion dynamics in these systems.

The optimal water number predicted by the DFT-RISM method were then used as inputs for direct AIMD simulations of ion confined in the MoS_2 channel. In particular, trajectories of ~50 ps were used to analyze the hydration structure of the solvated cations under confinement. Focus first on the atomic density distribution of ions and water perpendicular to the MoS_2 surface shown in Figure 2a and Figure S2 (parallel tests), we found that Li^+ and Na^+ prefer to stay in the center region of the MoS_2 channel whereas Rb^+ and Cs^+ exhibited a broaden and flat density across the channel. The density profile of K^+ behaved as a transition from Li^+/Na^+ to Rb^+/Cs^+ cases due to a small peak in the center region with a broaden non-zero density profile across the channel. This observation can be explained based on hydration effects associated with different cations. More specifically, Li^+ and Na^+ possess relatively higher hydration energy, and therefore they tend to reside in the center region of the channel to maintain their hydration shell. On the other hand, Rb^+ and Cs^+ have a lower hydration energy and are energetically more favorable to approach the MoS_2 channel wall due to a lower penalty for dehydration. Interestingly, this observation is also consistent with our early studies of ions confined in narrow carbon-based nanopores, despite that the previous results were obtained with implicit RISM solvation model.[35] Moreover, comparing the density distribution of Li^+ and Na^+ in Figure 2a, Na^+ tends to have higher density in the pore center than Li^+, while Li^+ showed a relatively flat distribution. This phenomenon was consistent to our previous study on the potential energy surface (PES) of cation in carbon nanopores, which reported that the Li^+-pore interaction has a smooth PES due to its small ionic size and highly stable

hydration. On the other hand, Na^+ is more constraint in the center of the pore due to its larger ionic radius compared to Li^+.[35]

The density profile of water shown in Figure 2b indicated that hydrogen atoms are closer to the MoS_2 surface than oxygens in all solutions. We note that the intensity of the first hydrogen peak near the surface is as high as that of oxygen, suggesting that the MoS_2 channel exhibits a more hydrophilic nature compared to a graphene surfaces shown in previous study.[36] We note that the hydrophilic nature of MoS_2 has also been suggested by early experimental studies, where the authors conclude that MoS_2 surface is intrinsically mildly hydrophilic, and it only becomes hydrophobic once it adsorbs hydrocarbons from ambient air.[37-38] We note that the nature of the hydrophilicity of the electrode materials may affect the surface capacitance and therefore the performance of the material for energy storage.[39-40] For instance, recent theoretical study by Jalali *et al.* indicated a significant impact of the surface hydrophilicity on the dipole orientation of confined water in 2D channels, leading to a "negative" dielectric constant in these nano-channels.[41] This concept of "negative" dielectric constant has also been used to explain the trend in the capacitive performance of alkaline metal cations in MXene electrodes by Sugahara *et al.*[42]

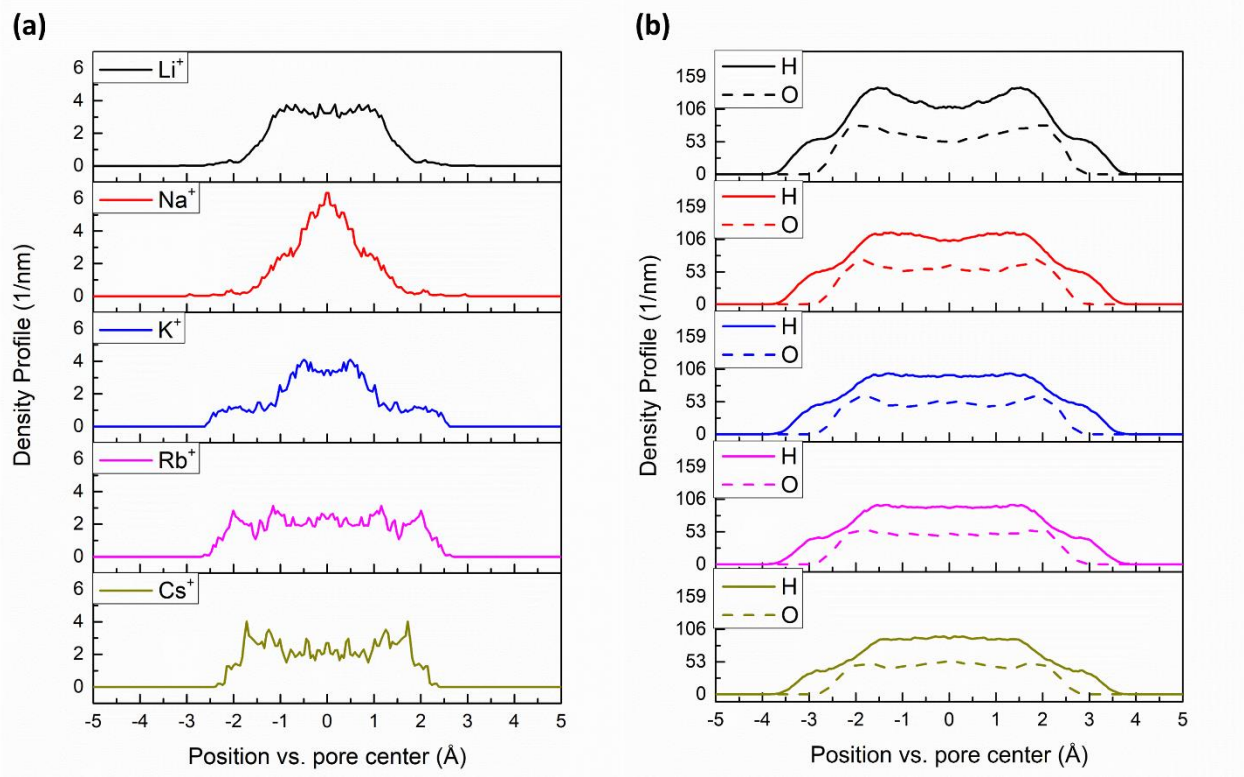

Figure 2. Density profiles of (a) cations and (b) H_2O along *z* axis. The position is referenced to the center of channel (*z*=0 Å).

Next, we utilized the radial distribution function (RDF) and oxygen-ion-oxygen angular distribution function (ADF) to characterize the hydration structure of the ions in solution. Specifically, to investigate the confinement effect on the hydration structure of different cations,

we computed the RDF (Figure 3a-e) and ADF (Figure 3f-j) of cation in MoS_2 channel and compared to those obtained for the bulk solutions. As shown by the dashed lines in Figure 3a-e for the RDF of bulk solution, we obtained the position of the first maximum (R_{max}) of $g_{M\text{-}O}$ at 1.95 Å, 2.31 Å, 2.80 Å, 2.98 Å, 3.15 Å, while corresponding value of the first minimum (R_{cutoff}) is 2.80 Å, 3.10 Å, 3.60 Å, 3.80 Å and 4.00 Å for Li^+, Na^+, K^+, Rb^+ and Cs^+ respectively (Table 1). The obtained peak positions were close to previously reported value via using classical and *ab initio* molecular dynamics within 0.2 Å (see Table 1). The discrepancy of valley position between our AIMD work and early CMD results is likely due to the numerical uncertainty in the calculation of the RDF (such as choice of bin size and number of involved trajectory), size limitation of simulation box and electronic quantum effects. We note that the position of the first local minimum in the RDF of the ions in bulk solution is used as the cutoff distance (R_{cutoff}) to compute the oxygen coordination number (CN) of ions in all systems. Comparing the RDF of cation in MoS_2 (solid lines in Figure 3a-e) and bulk solution (dashed lines in Figure 3a-e) in Table 1, Li^+, Na^+ and K^+ in MoS_2 showed nearly identical peak position to the bulk solution, while Rb^+ and Cs^+ showed a slight decreas of ~0.06-0.08 Å in the peak position, indicating the shrinkage of hydration shell under confinement.

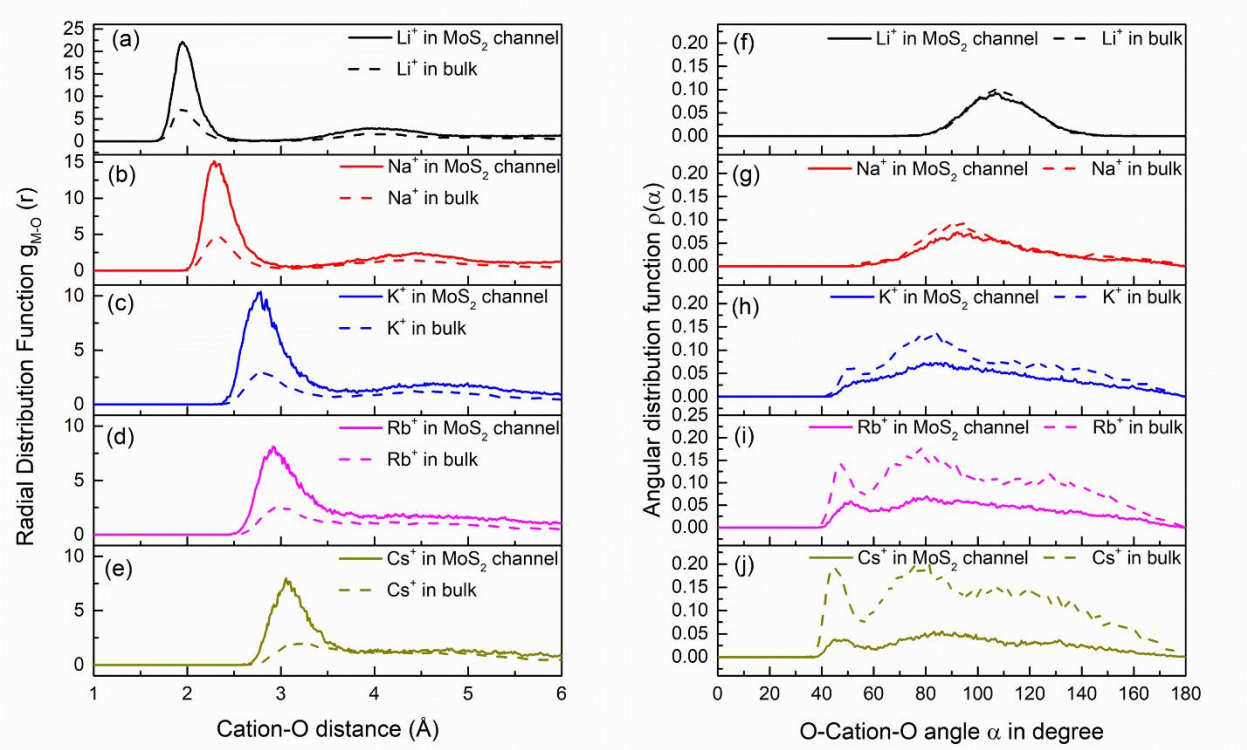

Figure 3. (a)-(e): Radial distribution function (RDF) of cation-oxygen in MoS_2 channel (solid line) and bulk (dashed line); (f)-(j): Angular distribution function (ADF) of O-M-O in MoS_2 (solid line) channel and bulk (dashed line).

Analysis of the ADF is also useful for investigating the hydration structure as it provides geometric information of the shape of the hydrated ions. In particular, a combination of the analysis

of the ADF (Figure 3f-j) and CN partition (Figure 4a-e), and visualization of the conformation of the hydrated ions (Figure 5) provided detailed structural information of hydration shell for different cations. The ADF computed for Li^+ in bulk solution shown in the dashed line in Figure 3f exhibited a symmetric peak centered at ~109°. This is an indicator of a tetrahedral shape of the hydration shell with four coordinated water molecules, as confirmed by the CN partition presented in Figure 4a and Figure 5f. With an increase in the cation size, cations in the bulk solution exhibited a peak shift to a smaller angle with an enhanced ADF intensity due to a higher CN. In addition, from the CN partition shown in Figure 4, we can correlate the calculated CN with the cation size. Specifically, the CN of Li^+ is almost solely dominated by 4, while the CN of Na^+ is dominated by 4 and 5 with a similar partition probability. On the other hand, K^+, Rb^+, Cs^+ exhibited a much more broaden CN partition of 5-8, 6-9, 7-10 respectively, consistent to the increased partition of a small coordination angle shown in Figure 3h-j. Overall, the average CNs of the cations in the bulk solution increased as the hydration energy decreases, yielding a value of 3.96, 4.67, 6.39, 7.65, 8.41 for Li^+, Na^+, K^+, Rb^+, Cs^+ respectively.

Comparing with the cations in the bulk solutions, the ADF calculated for those confined in the MoS_2 channel showed a strong decrease in the intensity except for Li^+ and Na^+in Figure 3f-j. As shown in Figure 3f, Li^+ exhibited nearly no change on the ADF (shape, location and height of peak), while Na^+ showed slightly decrease of the ADF value (Figure 3g). In contrast, other cations (K^+, Rb^+, Cs^+) showed a large decrease in the ADF value despite that the peak position of the ADF in small angle region (~50º and ~80º in Figure 3h-j) computed for these cations is barely changed in Figure h-j. Especially, the shape of ADF for K^+ (Figure 3h) changed from bimodal to unimodal due to the significant decrease of ADF intensity at ~50º and ~80º. This observation is due to the decrease in the number of counted coordination angle in the ADF analysis defined by equation (1) due to the confinement. In particular, from the calculated CN partition of cation in MoS_2 in Figure 4, the overall partition was found to shift to the lower CN side for most of the ions, leading to the decrease in the average CN. This is summarized in Table 1, where we obtained a value of 3.91, 4.31, 4.98, 5.00, 4.31 for confined Li^+, Na^+, K^+, Rb^+,Cs^+, respectively.

In addition, comparison of the hydration structure in MoS_2 (Figure 5a-e) and bulk (Figure 5f-j) showed that the intercalated Li^+ and Na^+ in the channel tends to retain the same hydration structure to that in bulk solution due to their strong hydration effect, while other ions lose 30%-50% hydration due to the confinement. Specifically, for the cations with a weak hydration (K^+, Rb^+, Cs^+), although their CN significantly decreased in the channel, we found that the ADF showed a similar shape and peak position to the bulk solutions (Figure 3h-j). Especially, the decrease of ADF for large cations (Figure 3h-i) mainly focus on the peak position in bulk (~50º and ~80º). This indicated a similar, but partially broken hydration geometry of these ions, as demonstrated further in Figure 5a-e and Figure 6. We note that a partially broken hydration shell of Rb^+ and Cs^+ leads to a direct contact of the bare ions with the MoS_2 wall, which impacts ion-pore polarization, interfacial charge transfer[35] and potentially their transport behavior.[43] In particular, a weakened hydration observed for the large cations under confinement could lead to enhanced transport, which in turn influences the capacitive performance. For instance, this enhanced transport of the large cations could be responsible for the observation that the capacitance of Rb^+ and K^+ are

significantly lower than Li^+ at low scan rates, but become similar at high scan rates for Ti_2CT_x electrodes.[42]

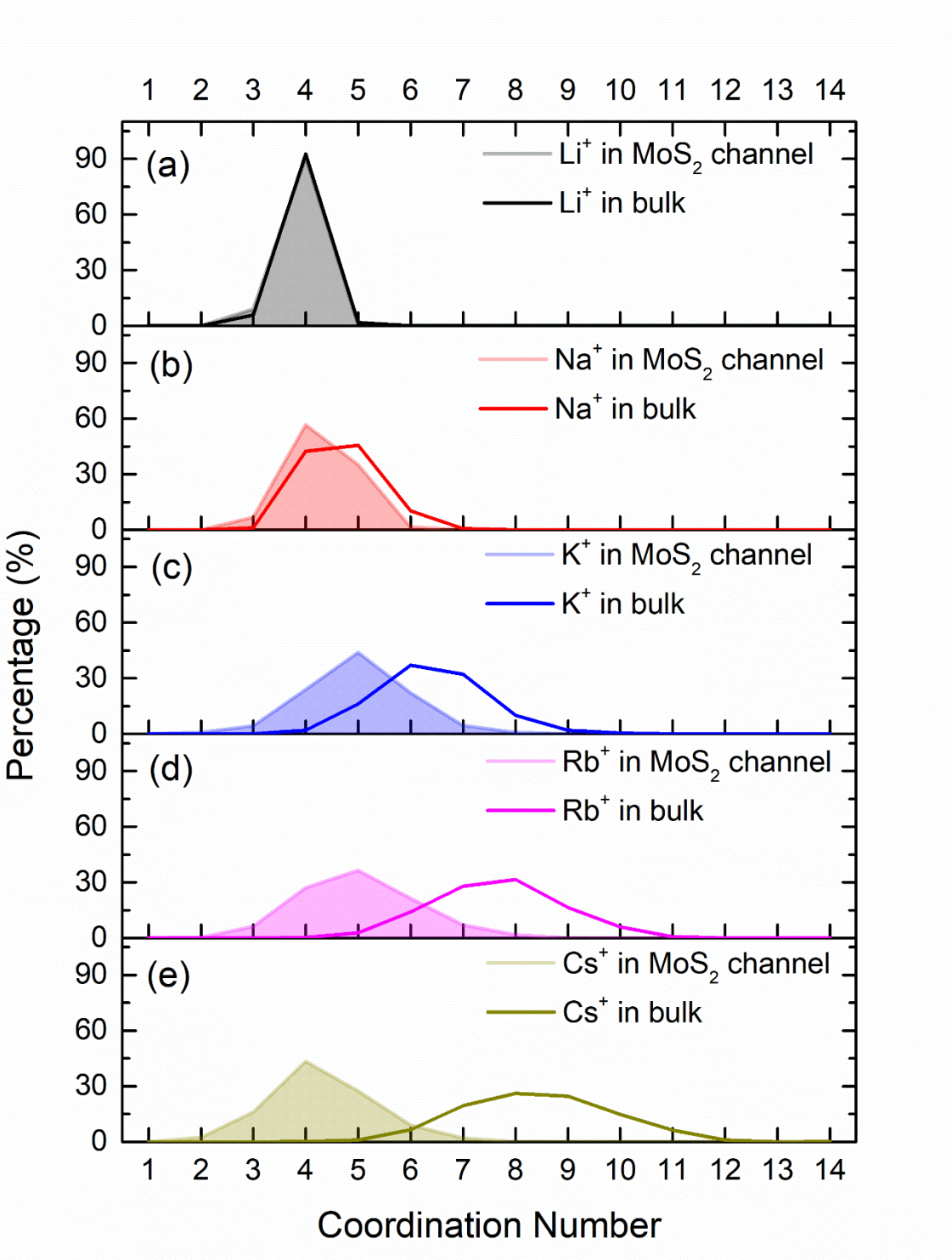

Figure 4. Probability partition of cation's coordination number (CN) with water in MoS_2 channel and bulk: (a) Li^+; (b) Na^+; (c) K^+; (d) Rb^+; (e) Cs^+.

Table 1. Summary of RDF peak position (R_{max}), RDF valley position (used as the R_{cutoff} for CN calculation) and average CN of alkaline metal cations in different systems as well as R_{max} values reported in early studies. (CMD refers to classical molecular dynamics; AIMD refers to the *ab initio* molecular dynamics)

System/Method	Property	Li^+	Na^+	K^+	Rb^+	Cs^+
Ion in bulk (this work) AIMD PBE at 400K	R_{max}	1.95 Å	2.31 Å	2.80 Å	2.98 Å	3.15 Å
	R_{cutoff}	2.80 Å	3.10 Å	3.60 Å	3.80 Å	4.00 Å
	CN	3.96	4.67	6.39	7.65	8.41
MoS_2 channel with optimal N_{water}	R_{max}	1.95 Å	2.30 Å	2.78 Å	2.92 Å	3.07 Å
	R_{cutoff}	2.78 Å	3.12 Å	3.70 Å	3.86 Å	3.91 Å
	CN	3.91	4.31	4.98	5.00	4.31
MoS_2 channel with N_{water} = 34	R_{max}	1.95 Å	2.29Å	2.77 Å	2.95 Å	3.11 Å
	R_{cutoff}	2.80 Å	3.12 Å	3.72 Å	4.08 Å	4.20 Å
	CN	3.91	4.20	5.26	5.34	5.66
MoS_2 channel with N_{water} = 23	R_{max}	1.97 Å	2.31 Å	2.74 Å	2.91 Å	3.07 Å
	R_{cutoff}	2.85 Å	3.22 Å	3.67 Å	3.99 Å	3.95 Å
	CN	3.93	4.34	4.64	5.13	4.31
Ion in bulk (reference/method)						
Ref. [44]/CMD	R_{max}				2.87 Å	3.12 Å
	CN				8.0	9.9
Ref. [45]/CMD	R_{max}	1.98 Å	2.46 Å	2.83 Å	2.94 Å	3.10 B
	CN					
Ref. [46]/AIMD PBE-D3	R_{max}	1.98 Å	2.41 Å	2.80 Å		3.17 Å
	CN	4.0	5.1	6.2		5.9
Ref. [47]/AIMD SCAN	R_{max}		2.51 Å	2.98 Å		
	CN					
Ref. [48]/AIMD B3LYP	R_{max}				2.99 Å	
	CN				6.31	

Finally, to explore the effect of water density on the hydration structure, we also investigated confined ions in MoS_2 filled with two extreme numbers of water molecules, i.e., N_{water}=34 and N_{water}=23, which correspond to the optimal water number of Li^+ and Cs^+, respectively. The calculated density profile of cation and water in Figure S3 and S4 showed consistent results to the optimal water number case. At both high and low water concentration, the density profile of small cations (Li^+ and Na^+) showed a typical peak in the center region, while large cations (Rb^+ and Cs^+) showed a relatively more broaden and flat distribution across the channel. In addition, as shown in Figure S5, we found that the water number has a little impact on the CN distribution of Li^+ and Na^+, while it has a much stronger influence on the CN of other cations. For instance, K^+ showed an obvious increase of partition at CN=3 and 4 when water number changed from 34 to 23. Similarly, the CN partition of Cs^+ showed an overall shift to the lower value with the water number decrease from 34 to 23. Although no large difference was observed for the ADF (Figure S6c-d), a distinctive increase in the position of the first maximum of the RDF calculated for Li^+ and Na^+, as shown in Figure S6a-b. This indicated that the hydration shell of Li^+ and Na^+ become more compact at a low water density. Overall, our calculations showed that this different sensitivity of the cations on the confined water density could be another factor that potentially affects their transport behavior.

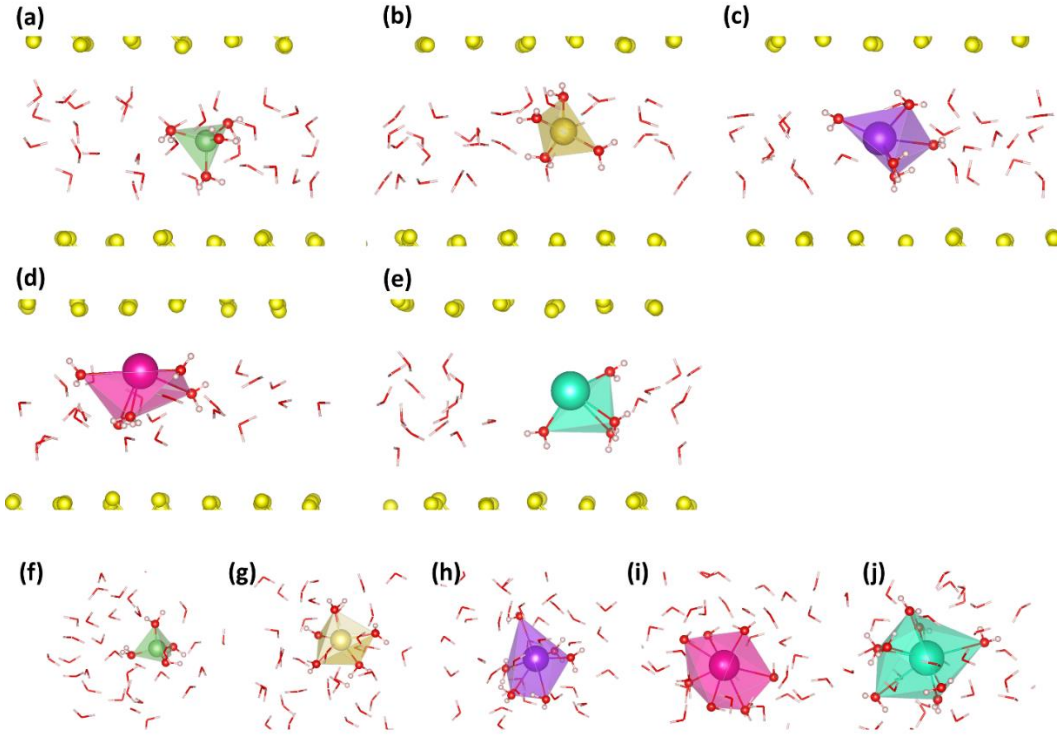

Figure 5. Snap shots of solvated cation and their coordinated water molecules in (a)-(e) MoS_2 channel and (f)-(j) bulk. Different ion in a-e and f-j follows the order Li^+, Na^+, K^+, Rb^+, Cs^+.

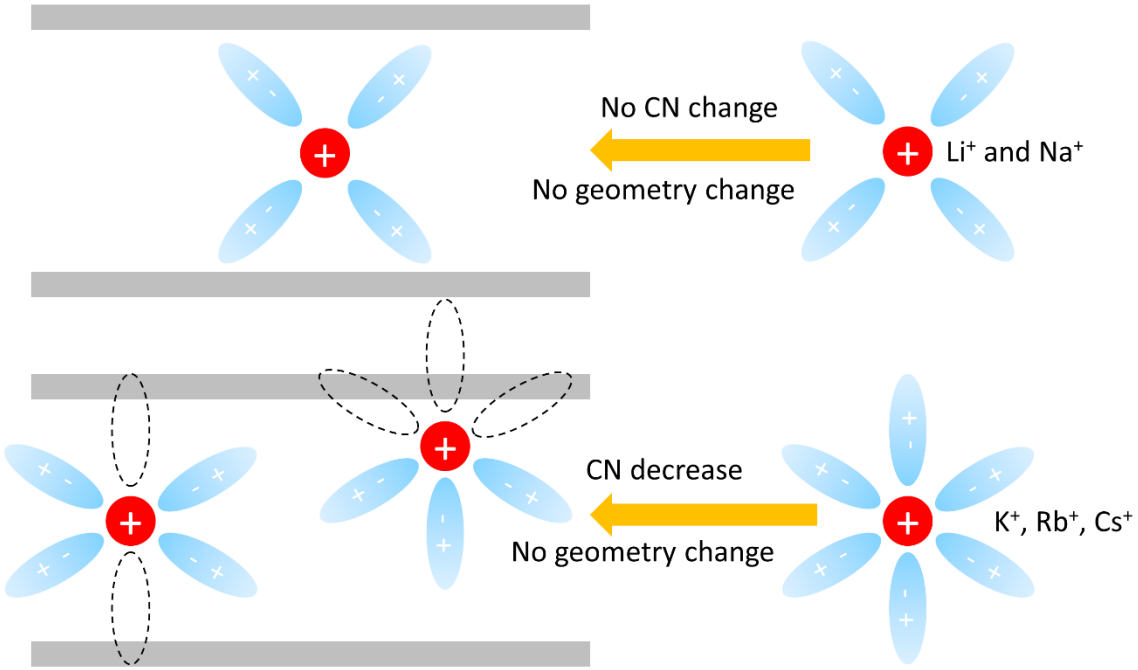

Figure 6. Schematic illustration of confinement effect on different alkaline metal cation.

Conclusion:

In this work, we combined the DFT-RISM and DFT-MD to study the confinement effect of the solvated alkaline metal cation in 1T-MoS_2 channel. Our DFT-RISM calculation showed that ions with a higher hydration energy are able to carry a larger number of water molecules into the MoS_2 channel, consistent with early experiments obtained for MXene channels. In addition, based on the optimal water number obtained from DFT-RISM calculations, we used explicit water molecules to simulate the solvated cation in MoS_2 channel and compared the simulation results to the bulk solution. Our statistical analysis of CN, RDF and ADF on MD trajectories indicated that: (i) Li^+ tends to retain the same hydration structure in MoS_2 channel and bulk solution with no sensitivity to the water density in channel; (ii) Na^+ shows a minor change on the hydration structure; and (iii) K^+, Rb^+ and Cs^+ showed significant change on hydration structure with distinct sensitivity to the water density in channel. Our simulations revealed atomistic details of confinement effects on different alkaline metal cations in the MoS_2 channel, which provide potential insights into the transport mechanism and ion dynamics in 2D materials in aqueous electrolytes.

Suplementary Material: Test of revPBE-D3 functional; cation density distribution from parallel MD tests; cation and water density distribution from AIMD simulation with 34 and 23 water molecules; distribution of CN from 34 and 23 water simulation; RDF and ADF from 34 and 23 water simulation.

Acknowledgement:

This work was performed under the auspices of the U.S. Department of Energy by Lawrence Livermore National Laboratory under Contract DE-AC52-07NA27344. The authors were supported as part of the Center for Enhanced Nanofluidic Transport, an Energy Frontier Research Center funded by the U.S. Department of Energy, Office of Science, Basic Energy Sciences under Award No. DE-SC0019112. CZ was also supported by the UCOP Project LFR-17-477237. YMW acknowledges the support of UCOP Project LFR-17-477237. Computational resources were awarded by the Lawrence Livermore National Laboratory Institutional Computing Grand Challenge Program.

Data Availability Statements:

The data that support the findings of this study are available from the corresponding author upon reasonable request.

Reference:

1. P. Biesheuvel and A. Van der Wal, J. Membr. Sci. **346**, 256 (2010).
2. B. Corry, J. Phys. Chem. B **112**, 1427 (2008).
3. S.-i. Jeon, H.-r. Park, J.-g. Yeo, S. Yang, C. H. Cho, M. H. Han and D. K. Kim, Energ. Environ. Sci. **6**, 1471 (2013).
4. S. Faucher, N. Aluru, M. Z. Bazant, D. Blankschtein, A. H. Brozena, J. Cumings, J. Pedro de Souza, M. Elimelech, R. Epsztein, J. T. Fourkas, A. G. Rajan, H. J. Kulik, A. Levy, A. Majumdar, C. Martin, M. McEldrew, R. P. Misra, A. Noy, T. A. Pham, M. Reed, E. Schwegler, Z. Siwy, Y. Wang and M. Strano, J. Phys. Chem. C **123**, 21309 (2019).
5. C. Largeot, C. Portet, J. Chmiola, P.-L. Taberna, Y. Gogotsi and P. Simon, J. Am. Chem. Soc. **130**, 2730 (2008).
6. G. Feng and P. T. Cummings, J. Phys. Chem. Lett. **2**, 2859 (2011).
7. D.-e. Jiang, Z. Jin and J. Wu, Nano. Lett. **11**, 5373 (2011).
8. R. K. Kalluri, D. Konatham and A. Striolo, J. Phys. Chem. C **115**, 13786 (2011).
9. H. Dai, Z. Xu and X. Yang, J. Phys. Chem. C **120**, 22585 (2016).
10. K. Krishnamoorthy, P. Pazhamalai, G. K. Veerasubramani and S. J. Kim, J. Power Sources **321**, 112 (2016).
11. E. G. da Silveira Firmiano, A. C. Rabelo, C. J. Dalmaschio, A. N. Pinheiro, E. C. Pereira, W. H. Schreiner and E. R. Leite, Adv. Energy Mater. **4**, 1301380 (2014).
12. M. Acerce, D. Voiry and M. Chhowalla, Nat. Nanotechnol. **10**, 313 (2015).
13. W. Hirunpinyopas, E. Prestat, S. D. Worrall, S. J. Haigh, R. A. Dryfe and M. A. Bissett, Acs Nano **11**, 11082 (2017).
14. W. Li, Y. Yang, J. K. Weber, G. Zhang and R. Zhou, Acs Nano **10**, 1829 (2016).
15. M. Heiranian, Y. Wu and N. R. Aluru, J. Chem. Phys. **147**, 104706 (2017).
16. N. Shpigel, M. D. Levi, S. Sigalov, T. S. Mathis, Y. Gogotsi and D. Aurbach, J. Am. Chem. Soc. **140**, 8910 (2018).
17. Y. Ando, M. Okubo, A. Yamada and M. Otani, Adv. Funct. Mater. **30**, 2000820 (2020).

18. S. Nishihara and M. Otani, Phys. Rev. B **96**, 115429 (2017).
19. P. Giannozzi, S. Baroni, N. Bonini, M. Calandra, R. Car, C. Cavazzoni, D. Ceresoli, G. L. Chiarotti, M. Cococcioni, I. Dabo, A. Dal Corso, S. de Gironcoli, S. Fabris, G. Fratesi, R. Gebauer, U. Gerstmann, C. Gougoussis, A. Kokalj, M. Lazzeri, L. Martin-Samos, N. Marzari, F. Mauri, R. Mazzarello, S. Paolini, A. Pasquarello, L. Paulatto, C. Sbraccia, S. Scandolo, G. Sclauzero, A. P. Seitsonen, A. Smogunov, P. Umari and R. M. Wentzcovitch, J. Phys.: Condens. Matter **21**, 395502 (2009).
20. J. P. Perdew, K. Burke and M. Ernzerhof, Phys. Rev. Lett. **77**, 3865 (1996).
21. D. Hamann, Phys. Rev. B **88**, 085117 (2013).
22. A. Kovalenko and F. Hirata, J. Chem. Phys. **110**, 10095 (1999).
23. M. Matsugami, N. Yoshida and F. Hirata, J. Chem. Phys. **140**, 104511 (2014).
24. L. Martínez, R. Andrade, E. G. Birgin and J. M. Martínez, J. Comp. Chem. **30**, (2009).
25. Y. Marcus, J. Chem. Soc., Faraday Trans. **87**, (1991).
26. G. Kresse and J. Furthmüller, Phys. Rev. B **54**, 11169 (1996).
27. G. Kresse and D. Joubert, Phys. Rev. B **59**, 1758 (1999).
28. S. Nosé, J. Chem. Phys. **81**, 511 (1984).
29. N. Shuichi, Prog. Theor. Phys. Suppl. **103**, 1 (1991).
30. D. Bylander and L. Kleinman, Phys. Rev. B **46**, 13756 (1992).
31. T. A. Pham, T. Ogitsu, E. Y. Lau and E. Schwegler, J. Chem. Phys. **145**, 154501 (2016).
32. E. Schwegler, J. C. Grossman, F. Gygi and G. Galli, J. Chem. Phys. **121**, 5400 (2004).
33. J. C. Grossman, E. Schwegler, E. W. Draeger, F. Gygi and G. Galli, J. Chem. Phys. **120**, 300 (2004).
34. M. Brehm and B. Kirchner, J. Chem. Inf. Model. **51**, 2007 (2011).
35. C. Zhan, F. Aydin, E. Schwegler, A. Noy and T. A. Pham, ACS Appl. Nano Mater. **3**, 9740 (2020).
36. G. Cicero, J. C. Grossman, E. Schwegler, F. Gygi and G. Galli, J. Am. Chem. Soc. **130**, 1871 (2008).
37. A. Kozbial, X. Gong, H. Liu and L. Li, Langmuir **31**, 8429 (2015).
38. J. He, G. Hartmann, M. Lee, G. S. Hwang, Y. Chen and A. Manthiram, Energ. Environ. Sci. **12**, 344 (2019).
39. D. J. Bonthuis, S. Gekle and R. R. Netz, Langmuir **28**, 7679 (2012).
40. F. o. Dehez, L. Delemotte, P. Kramar, D. Miklavčič and M. Tarek, J. Phys. Chem. C **118**, 6752 (2014).
41. H. Jalali, F. Khoeini, F. M. Peeters and M. Neek-Amal, Nanoscale **13**, 922 (2021).
42. A. Sugahara, Y. Ando, S. Kajiyama, K. Yazawa, K. Gotoh, M. Otani, M. Okubo and A. Yamada, Nat. Commun. **10**, 1 (2019).
43. H. Zhu, Y. Xu, Y. Yan, J. Xu and C. Yang, Langmuir **36**, 13613 (2020).
44. D. Z. Caralampio, J. M. Martínez, R. R. Pappalardo and E. S. Marcos, Phys. Chem. Chem. Phys. **19**, 28993 (2017).
45. Q. A. Besford, M. Liu and A. Gray-Weale, Phys. Chem. Chem. Phys. **18**, 14949 (2016).
46. X. Wang, D. Toroz, S. Kim, S. L. Clegg, G.-S. Park and D. Di Tommaso, Phys. Chem. Chem. Phys. **22**, 16301 (2020).
47. T. T. Duignan, G. K. Schenter, J. L. Fulton, T. Huthwelker, M. Balasubramanian, M. Galib, M. D. Baer, J. Wilhelm, J. Hutter and M. Del Ben, Phys. Chem. Chem. Phys. **22**, 10641 (2020).
48. A. Boda and S. M. Ali, J. Mol. Liq. **179**, 34 (2013).